NeuroImage 244 (2021) 118611

Contents lists available at ScienceDirect

NeuroImage

journal homepage: www.elsevier.com/locate/neuroimage

The connectome spectrum as a canonical basis for a sparse representation of fast brain activity

Joan Rué-Queralt[a,b,*], Katharina Glomb[a], David Pascucci[c], Sébastien Tourbier[a], Margherita Carboni[d,e], Serge Vulliémoz[e], Gijs Plomp[b], Patric Hagmann[a]

[a] Connectomics Lab, Department of Radiology, Lausanne University Hospital and University of Lausanne (CHUV-UNIL), Lausanne, Switzerland
[b] Perceptual Networks Group, Dept. of Psychology, University of Fribourg, Fribourg, Switzerland
[c] Signal Processing Lab 2, EPFL, Lausanne, Switzerland
[d] EEG and Epilepsy, Neurology, University Hospital of Geneva and University of Geneva, Geneva, Switzerland
[e] Functional Brain Mapping Lab, Department of Fundamental Neurosciences, University of Geneva, Geneva, Switzerland

A B S T R A C T

The functional organization of neural processes is constrained by the brain's intrinsic structural connectivity, i.e., the connectome. Here, we explore how structural connectivity can improve the representation of brain activity signals and their dynamics. Using a multi-modal imaging dataset (electroencephalography, structural MRI, and diffusion MRI), we represent electrical brain activity at the cortical surface as a time-varying composition of harmonic modes of structural connectivity. These harmonic modes are known as connectome harmonics. Here we describe brain activity signal as a time-varying combination of connectome harmonics. We term this description as the connectome spectrum of the signal. We found that: first, the brain activity signal is represented more compactly by the connectome spectrum than by the traditional area-based representation; second, the connectome spectrum characterizes fast brain dynamics in terms of signal broadcasting profile, revealing different temporal regimes of integration and segregation that are consistent across participants. And last, the connectome spectrum characterizes fast brain dynamics with fewer degrees of freedom than area-based signal representations. Specifically, we show that a smaller number of dimensions capture the differences between low-level and high-level visual processing in the connectome spectrum. Also, we demonstrate that connectome harmonics capture more sensitively the topological properties of brain activity. In summary, this work provides statistical, functional, and topological evidence indicating that the description of brain activity in terms of structural connectivity fosters a more comprehensive understanding of large-scale dynamic neural functioning.

1. Introduction

The brain is a large biological network of interconnected neural populations. Given the vast number of neural populations, at the macroscopic level, the activity of the brain is commonly studied using a parcellation. The choice of brain parcellation into areas of interest reflects the underlying assumption on how large populations of neurons cluster together, and typical clustering models are anatomical (Desikan et al., 2006), functional (Gordon et al., 2016; Yeo et al., 2011), structural (Fan et al., 2016) or multi-modal (Glasser et al., 2016). Considering the entire brain, its activity can be represented as a trajectory over time in a high-dimensional coordinate system where each dimension represents the activity of a specific brain area. Even though these brain areas are commonly regarded as independent units, they synchronize among them according to their connectivity (Vincent et al., 2007). In this work, we focus on local measures of cortical electrical activity as measured by source reconstructed electroencephalography (EEG).

In particular, we assume that brain activity is defined on top of the structural connectivity (SC), i.e., the connectome (Hagmann, 2005; Sporns et al., 2005). The SC can be conceptualized as a graph in which the nodes are defined as gray matter brain areas using a reference atlas and a parcellation (see Fig. 1C). The edges of this graph reflect some property of the estimated white matter connectivity (number of fibers, their average length or mean fractional anisotropy), which is estimated using diffusion magnetic resonance imaging (Hagmann et al., 2008) (dMRI, see Fig. 1D). When analyzing any signal, the graph upon which it is defined allows us to draw observations from a global perspective (as opposed to local). For example, in a movie, the graph upon which the image is defined consists of a two-dimensional grid, in which pixels are connected to their four nearest neighbors. This graph allows us to determine the relevance of a pixel value within the image at a given time-point, i.e., data from neighboring pixels can be seen as redundant, if both pixels encode a piece of background, or very significant, if they are forming an edge belonging to a contour.

When analyzing a signal of which the underlying domain is known and can be defined by a graph, such as the structural connectivity, one can decompose the signal as the sum of graph Laplacian eigenvectors. This operation is known as the graph Fourier transform

* Corresponding author at: Connectomics Lab, Department of Radiology, Lausanne University Hospital and University of Lausanne (CHUV-UNIL), Lausanne, Switzerland.
E-mail address: Joan.Rue-Queralt@chuv.ch (J. Rué-Queralt).

https://doi.org/10.1016/j.neuroimage.2021.118611.
Received 26 April 2021; Received in revised form 28 July 2021; Accepted 20 September 2021
Available online 21 September 2021.
1053-8119/© 2021 The Authors. Published by Elsevier Inc. This is an open access article under the CC BY license (http://creativecommons.org/licenses/by/4.0/)

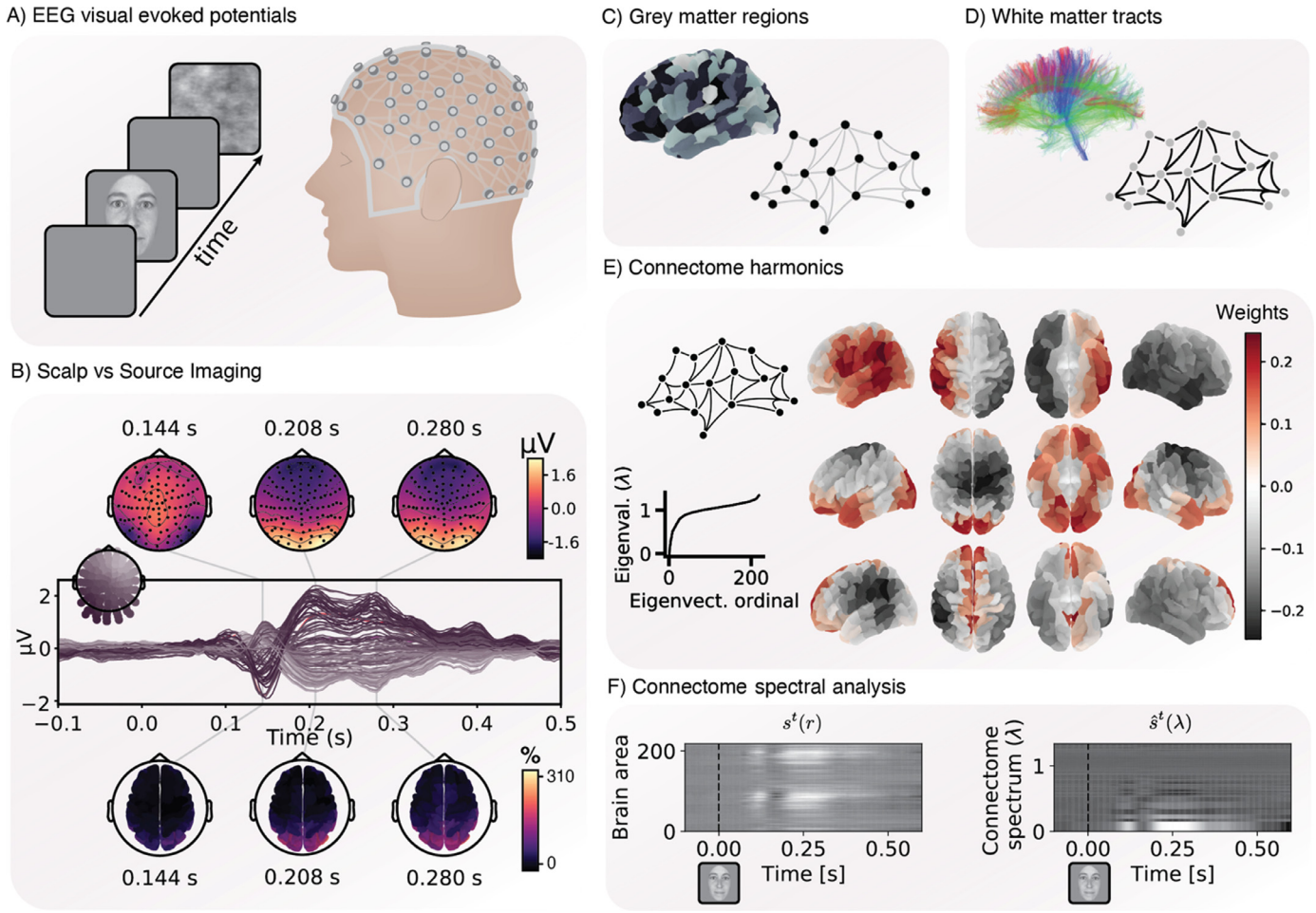

Fig. 1. Connectome harmonics for visual evoked potentials. (A) The visual evoked potentials' experimental design consisted in the presentation of two types of stimuli: faces and scrambled-faces. The face images were taken from an openly available dataset (Pascucci et al., 2021) and cropped with a Gaussian kernel to smooth the borders. For each one of the 19 participants, approximately 200 trials for each condition were recorded and aligned at the onset of the stimulus presentation. (B) Scalp patterns before, and after the face stimulus is presented (at 0 ms) (generated with the visualization tool of MNE v0.21), and the source reconstruction of the stimulus evoked activity. (C) gray matter areas defined by an anatomical parcellation define the nodes of the brain graph. (D) The estimated white matter tracts from diffusion MRI define the connectivity strength of the edges of the graph. (E) From the constructed graph, we perform the graph Laplacian eigendecomposition and obtain a graph spectrum, consisting of a set of eigenvalues and a set of eigenvectors, the former ones termed graph spectrum, and the later termed graph or connectome harmonics. A few more examples of connectome harmonics are shown in Fig. S1. (F) The source reconstructed time-series signal represented in each brain area r (left plot, $s^t(r)$) or in each connectome spectrum corresponding to each graph Laplacian eigenvalue λ (right plot, $\hat{s}^t(\lambda)$). In the connectome spectrum plot, the rows' height corresponds to the value of λ.

(Shuman et al., 2013) (GFT). In the case of the brain, we define connectome spectral analysis as the connectome graph Fourier Transform of the brain activity signal:

$$\hat{\mathbf{s}}^t(\lambda) = GFT\left(\mathbf{s}^t(r)\right) = \mathbf{U}^{\mathrm{T}}\mathbf{s}^t(r), \tag{1}$$

where $\mathbf{s}^t(r)$ represents the electrical activity estimated at each brain region r at time t, and the columns of $\mathbf{U}$ contain the connectome Laplacian eigenvectors $\{\mathbf{u}_i\}$, referred to as connectome harmonics (Atasoy et al., 2016). The signal's connectome spectrum $\hat{\mathbf{s}}^t(\lambda)$ defines the participation of each connectome harmonic in the signal $\mathbf{s}^t(r)$ (Huang et al., 2016; Glomb et al., 2020) (see Figs. 1E–F and S1). The GFT is analogous to the discrete Fourier transform for temporal signals and to the two-dimensional Fourier transform for images (see Fig. S1 for illustration). Connectome harmonics $\{\mathbf{u}_i\}$ are ordered by their associated connectome graph Laplacian eigenvalues $\{\lambda_i\}$ which quantify their smoothness (in terms of Dirichlet energy Belkin and Niyogi 2001). The smoothness of each harmonic can be understood as a graph frequency (see Fig. S1). Low-frequency connectome harmonics capture smooth signal gradients over the structural connectivity graph, for example capturing the left-right, anterior-posterior, ventral-to-dorsal and the medial-peripheral axes (Atasoy et al., 2016). By contrast, high-frequency harmonics capture irregular patterns over the connectivity graph in space (see Fig. S1 for illustration).

The structure-function relationship is an unresolved topic in neuroscience (Vincent et al., 2007; Robinson et al., 2003; Deco et al., 2008; Avena-Koenigsberger et al., 2018; Seguin et al., 2020), and recently, several studies have explored potential applications of connectome spectral analysis (see Lioi et al. 2021 for a review). Characterizing brain function by means of its underlying graph is motivated by the fact that brain activity is constrained by, and coupled through its structural connectivity (Glomb et al., 2020; Sorrentino et al., 2021). When functional interactions follow structural connections, as in the case of brain activity, the signal is represented in the smoothest subset of connectome harmonics, and thus, it can be reconstructed with a sparse signal representation (Glomb et al., 2020; Abdelnour et al., 2018). Exploiting the underlying signal's graph might not only improve the statistical properties of the signal, but it could also provide mechanistic information on how signals propagate. In this sense, connectome harmonics have been

theoretically proposed as a mechanism for macroscopic brain activity, allowing nested functional segregation and integration across multiple spatio-temporal scales (Wang et al., 2019).

Even though connectome harmonics seem a promising tool for studying whole-brain activity, a comprehensive empirical evaluation of the properties of the signal's connectome spectrum is lacking. In this work, we characterized the advantages of connectome harmonics as a coordinate system for representing the fast-evolving brain-wide activity signals at the cortical surface estimated from EEG recordings. We report some evidence suggesting the advantages of the connectome spectrum representation in three different aspects: the statistical, the functional, and the topological properties of the signal. We first show that during visual evoked brain activity, the EEG signal estimated at the cortical surface can be represented more compactly by its connectome spectrum than by its traditional area-based signal representation. The connectome spectrum, which is a model-based representation of the signal, performs equally or better in terms of compactness than traditional data-driven approaches such as PCA and ICA. Importantly, the compactness of the signal's connectome spectrum is specific to the connectivity structure, rather than to the graph spectral decomposition properties. Then, we demonstrate that the representation of the signal on its connectome spectrum automatically characterizes brain activity dynamics in terms of the signal broadcasting profile, revealing integration and segregation regimes of brain processing, which follow consistent dynamics across participants. Finally, we provide evidence that connectome harmonics capture the functional aspects of visual perception with fewer degrees of freedom than isolated brain areas. These advantages extend to topological properties of the signal and their fast temporal dynamics. After presenting these three types of evidence, we propose the connectome spectrum as a canonical basis for the representation of large-scale brain activity dynamics.

2. Results

2.1. A sparse basis for large-scale brain activity

Coordinate systems in which data are compactly represented are advantageous because they summarize the data well, and they provide robustness to small variations such as noise (Baraniuk et al., 2010). Furthermore, if brain activity admits a sparse signal representation, i.e., a transformation that describes the signal with only a few non-zero valued elements, it means that the underlying process has a limited number of parameters that we are able to estimate. The compactness of a signal indicates how compressible it is, and gives us an estimation on its sparsity (Candes and Davenport, 2013). In the present work, brain activity signal was recorded in visual evoked potential experiments using high-density EEG, and reconstructed at the cortical surface (see Fig. 1A,B). Using an anatomical parcellation, the single-trial cortical time-courses were parcellated into 219 areas (Cammoun et al., 2012) using the method introduced in (Rubega et al., 2019). We estimated the sparsity (in terms of signal compactness) of the brain activity in the usual brain area-based signal representation $\mathbf{s}^t(r)$ and in its connectome spectrum $\hat{\mathbf{s}}^t(\lambda)$ (Glomb et al., 2020), and we compared them.

The compactness of the evoked signal in each coordinate system was quantified by means of signal compression performance (inspired from (Grassi et al., 2017)). Signal compression was performed by replacing the signal values (and its spectrum coefficients) with magnitudes smaller than the p-th percentile with zeros (and performing the corresponding inverse GFT on the resulting coefficients in the case of the signal's connectome spectrum). The compactness for each p-th percentile was then defined as the Pearson correlation between the original and the compressed signal on the one hand, and as one minus the reconstruction error (see section *Methods: Analysis of Compactness*, Fig. 2A,B) on the other hand. In this way, the compression analysis collapsed time and produced only a scalar value for each compression percentile p. The results show that the thresholding performed in the connectome spectral

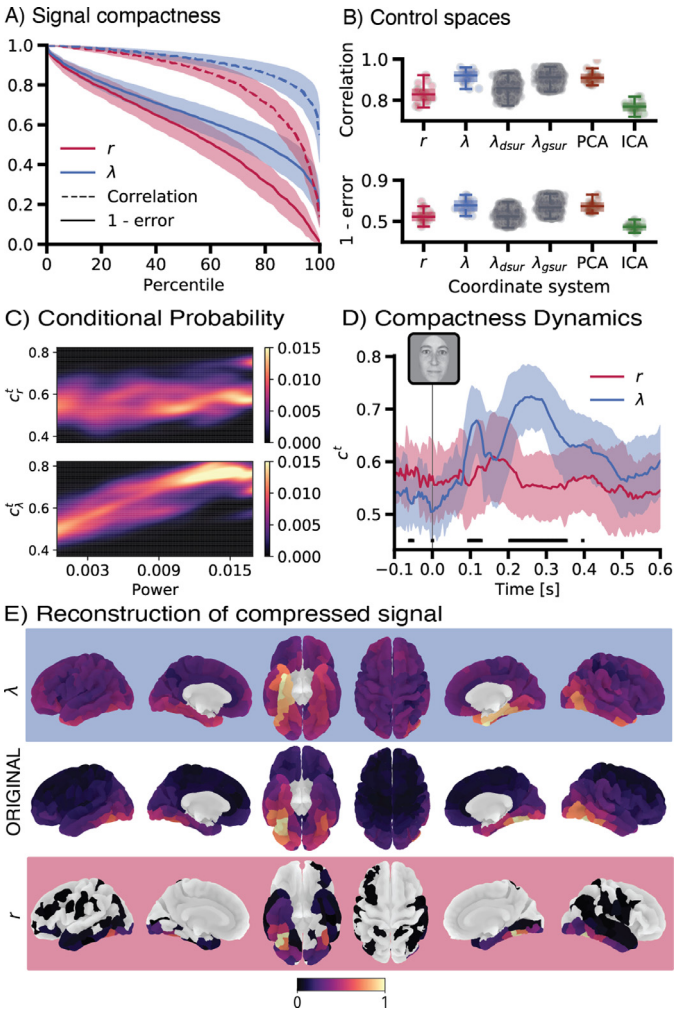

Fig. 2. Signal compactness in different coordinate systems of signal representation. (A) Signal compactness measured by two distance metrics between original and compressed signals: compression correlation (dashed line) and reconstruction error (continuous line) (see *Methods: Analysis of compactness*). The signal compression was performed at all integer percentiles from 1 to 100 for the signal represented by brain areas (r) and for the signal represented by connectome harmonics (λ), i.e., the signal's connectome spectrum. (B) Signal average compactness (mean across percentiles). It was computed for different controls (see *Methods*): λ_{dsur}, harmonics of degree-preserving surrogate connectomes; λ_{gsur}, harmonics of geometry-preserving surrogate connectomes; PCA, principal components from principal component analysis; and ICA, independent components from independent component analysis. See Fig. S2 for statistical significance tests of the differences among coordinate systems. Each data-point shows the mean compactness for each subject, and the boxplot indicates the median, quartiles and 5–95th percentiles of the subjects' distribution. (C) Conditional probability of the compactness dynamics c^t (shown in (D)). It is conditioned by the power of the signal at the same time-point (see *Methods: Conditional probabilities*) for either the area and the connectome harmonics' activity. (D) Compactness dynamics c^t. It was computed at each time-point as the compression reconstruction performance (1 - reconstruction error) averaged across percentiles (see *Methods: Analysis of compactness*), and informed about the number of active dimensions in time (i.e., a proxy of its sparsity). At each time-point, a Wilcoxon Rank-sum two-sided test was performed, and those time-points with significant p-value are indicated with black rectangular boxes (Bonferroni corrected for multiple comparisons). (E) Visual illustration on the brain surface of the effect of compressing a signal in different coordinate systems. The signal was compressed at 95-th percentile in each coordinate system (only 11 out of 219 dimensions are non-zero). For the area-based signal representation, the signal is shown right after being compressed. For the connectome spectrum of the signal, the compressed activation coefficients were mapped back to the original atlas-based coordinates. The error bars in this figure show the mean and standard deviation of the distribution across subjects.

domain achieved greater signal compactness than in the area-based coordinates ($p < 0.001$, Wilcoxon Rank-sum two-sided test, corrected for multiple comparisons via Bonferroni, Fig. S2A,B). This result indicates that $\hat{\mathbf{s}}^t(\lambda)$ is sparser than $\mathbf{s}^t(r)$, meaning that the evoked activity is described with fewer connectome harmonics than brain areas. The idea that the connectome spectrum of the signal is sparse is illustrated by the fact that we can reconstruct more than 50% of the explained variance of the signal after compressing down to just 5% of its connectome spectrum content.

For validation, we tested if the improved compression capacity was related to the structural connectivity graph capturing the mechanisms underlying brain activity dynamics, and not to general decomposition properties of the graph Laplacian. To this end, we performed a non-parametric statistical analysis by measuring the compactness of the signal represented by degree-preserving surrogate connectome harmonics and by geometry-preserving surrogate harmonics (Roberts et al., 2016) (see *Methods: Surrogate harmonics*). Briefly, degree-preserving surrogates generate random networks that preserve the connectivity degree distribution. Instead, geometry-preserving surrogate harmonics preserve the connectivity pattern while shuffling the connection weights. Interestingly, degree-preserving surrogates compress the signal slightly better than its area-based representation ($p < .01$ for correlation, $p > .05$ for reconstruction error, Wilcoxon Rank-sum two-sided test, corrected for multiple comparisons via Bonferroni, see Figs. 2B and S2A,B), suggesting that part of the improved performance is due to the decomposition properties of the graph Laplacian. Compared to the degree-preserving surrogates' compactness, the compactness of the signal's connectome spectrum was significantly higher, both in terms of signal correlation and reconstruction error ($p < .001$). However, the results indicate that the compactness performance is not significantly different between the structural connectome and its geometry-preserving surrogates ($p > .05$). These results show that is the actual spatial embeddedness of the connectome graph what drives the observed compression of the brain activity signal.

It is worth noting that signal decomposition techniques are usually data-driven (based on the statistical properties of the signal), such as in the case of Principal Component Analysis (PCA) or Independent Component Analysis (ICA). In contrast to these techniques, the connectome spectral decomposition provided by the connectome GFT is model-driven, as brain activity is modeled as a weighted sum of structural connectivity gradients. Fig. 2B assesses the compression properties of these well-known methods to benchmark the performance of connectome harmonics. It shows that connectome spectral analysis compares similarly to PCA in terms of correlation and reconstruction error, but it always outperforms ICA (see Fig. S2C,D; $p < .001$, Wilcoxon Rank-sum two-sided test, corrected for multiple comparisons via Bonferroni). These results suggest that connectome harmonics capture well the variance of the stimulus-evoked brain activity, and more specifically, that they compare favorably with commonly-used data-driven decomposition methods.

2.2. Compactness dynamics

Visual evoked potentials have a highly temporal non-stationary nature; therefore, the sparsity of the signal can be expected to change in time. For this reason, we assessed the dynamical properties of the signal in the coordinate system defined by the connectome harmonics. We hypothesized that the fast dynamics of the visual evoked activity should be reproducible across participants if the signal's connectome spectrum ($\hat{\mathbf{s}}^t(\lambda)$) captured relevant features. We used the compactness dynamics (c^t), defined as the reconstruction error of the compressed signal at a given time-point, averaged across all percentiles (*Methods: Analysis of compactness*), as a proxy of the number of active dimensions at each time-point, i.e., as the sparsity dynamics of the signal (Fig. 2D). The motivation behind this analysis is to reveal those time-points during which brain activity can be described by very few connectome harmonics, i.e., a sparse spectrum.

We first studied the dependency of the connectome spectral compactness on the power of the signal, to assess whether the activation of connectome harmonics was not trivial. We analyzed the relationship between the signal compactness and the total energy of the signal by means of the conditional probability $P(c^t | \| \cdot \|_2)$ (*Methods: Conditional probabilities*), for "$\cdot$" representing $\mathbf{s}^t(r)$ or $\hat{\mathbf{s}}^t(\lambda)$. The conditional probability showed a strong linear tendency, with an increase in the power of the signal positively correlated to the activation of a few connectome harmonics (see Fig. 2C). This result suggests that connectome spectrum compactness is non-randomly distributed in time, and can be partially explained by the dynamics of the power of the signal. In other words, this dependency indicates that in moments of high power the signal is concentrated in just few harmonics. When analyzing the area-based signal $\mathbf{s}^t(r)$, however, we did not find such a relationship, indicating that the power of the signal $\mathbf{s}^t(r)$ does not depend on the number of active areas.

To test whether connectome harmonics can characterize fast, functionally specific processes, we used visual-evoked potentials (VEP) to face presentation. Face-specific processes are well-studied and can be primarily localized to the Fusiform gyrus (Kanwisher et al., 1997), but are known to also involve occipital, parietal and orbitofrontal areas (Haxby et al., 2000; Gauthier et al., 2000; Rolls, 2007). They also have a specific temporal signature in terms of temporal localization (at around 170 ms after the stimulus is presented) (Plomp et al., 2010; Bentin et al., 1996). The compactness dynamics of connectome harmonics (c^t_λ) of the evoked signal revealed different regimes of visual processing (Fig. 2D).

At time zero (0 ms), the visual stimulus was presented and the brain signal associated with stimulus processing quickly built up, becoming more compact in both the connectome harmonic and area-based signal representation. This increased compactness was significantly larger for the connectome spectrum in three time-windows ([96–128 ms, 204–352 ms, 396–400 ms], $p < .05$, Wilcoxon Rank-sum two-sided test, corrected for multiple comparisons via Bonferroni). The increased compactness indicates that during these time windows, the variance of the signal was captured by fewer number of harmonics than number of brain areas. This result suggests that the constitution of the signal during those time-points is shaped by the activity of a limited number of connectome harmonics rather than the activity of isolated brain regions.

During pre-stimulus time, the evoked signal consists of the average activity across many non-aligned trials, and thus, can be regarded as residual noise. This noise should be ideally evenly distributed across dimensions. For this reason, the noisy signal during pre-stimulus time was not compressible in any coordinate system. However, such noise was more evenly distributed in the signal's connectome spectrum, and thus, significantly less compact ($p < .05$, Monte-Carlo simulations (1000 per time-point), corrected for multiple comparisons via Bonferroni, see *Methods: Statistical Analysis*), suggesting connectome harmonics as a robust representation against noise.

At this point, the reader might think that a compact signal might not be a good signal, but instead misses crucial information. To guarantee that the increased compactness of the signal does not come at the expense of destroying parts of the signal that are known to be relevant, we next focused only on two well-known spatio-temporal patterns: face processing in the ventral stream at 170 ms, and motion processing in the dorsal stream at 150 ms (see *Methods: EEG* and Supplementary text S1). For simplicity, reconstruction error and correlation after compression were estimated for three visual systems: ventral, dorsal and the group of early visual areas (see Fig. S3). The only significant differences in the compactness properties of $\mathbf{s}^t(r)$ and its connectome spectrum $\hat{\mathbf{s}}^t(\lambda)$ were found in motion perception at 150 ms ($p < .05$, corrected for multiple comparisons via Bonferroni), for which compactness was better in the connectome spectrum $\hat{\mathbf{s}}^t(\lambda)$. These results indicate that the connectome harmonic representation of the signal does not underestimate the part of the signal known to be functionally relevant.

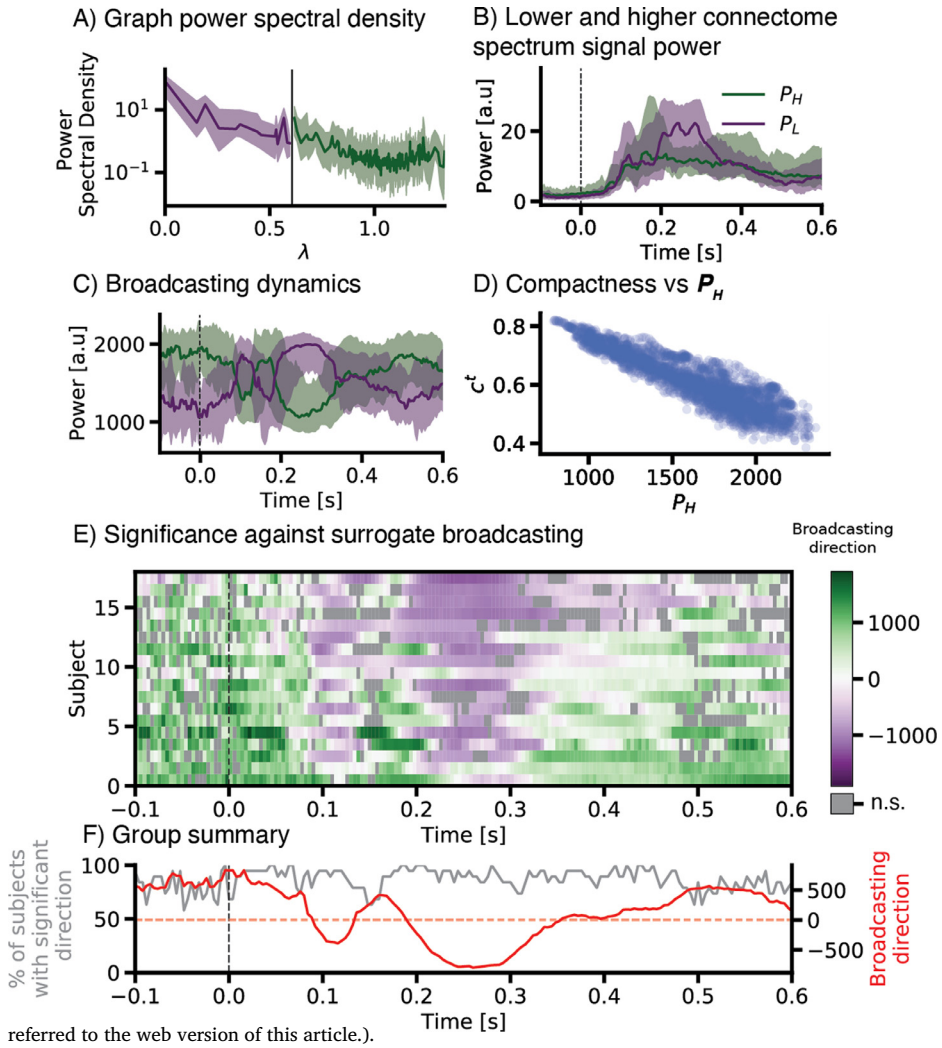

Fig. 3. Signal broadcasting profile. (A) Graph power spectral density across time. It was computed as the power in each connectome harmonic during the whole time-series (see *Methods: Graph spectrum dichotomization*). The power spectral density was then divided into two halves of equal cumulative power. (B) The energy of the brain activity signal contained in each of these two ends of the connectome spectrum was computed for each time-point: P_L^t, the energy concentrated in the lowest-end of the spectrum, associated with integration processes, and P_H^t, the energy concentrated in the highest-end of the spectrum, associated with brain activity segregation, respectively. (C) The time-courses in (B) were normalized by the power of the signal at each time-point, illustrating the normalized contribution across time to the total power of the signal. By definition, these time courses profile the brain activity broadcasting profile into integration and segregation dynamics. (D) The normalized P_H^t (segregation) at each time-point (shown in (C)) was compared to the connectome spectrum compactness dynamics (c^t, previously shown in Fig. 2D). (E) The significance of the broadcasting direction (here summarized as $P_H^t - P_L^t$) was tested against the broadcasting direction in degree-preserving surrogate connectomes (see *Methods: Broadcasting significance test*). For each subject, the non-significant time-points are colored in gray. Green colored time-points indicate a broadcasting profile dominated by segregation. (F) The group summary of (E) is represented by two time-resolved metrics: i) the percentage of subjects with a significant broadcasting direction (in gray) and the mean broadcasting direction across subjects. The continuous lines and the shaded area in the plots of this figure show the mean and standard deviations of the distribution across all subjects (For interpretation of the references to color in this figure legend, the reader is referred to the web version of this article.).

2.3. Integration and segregation dynamics during visual perception

Low-frequency harmonics (i.e., the connectome Laplacian eigenvectors corresponding to the smallest eigenvalues) define smooth gradients of structural connectivity. Assuming that the brain activity propagates through the structural connectivity (Avena-Koenigsberger et al., 2018), we can interpret low-frequency harmonics as integrative patterns, i.e., patterns of brain activity in which sets of neighboring brain regions show strong long-range coupling (in graph space). Conversely, high-frequency harmonics reflect short-range coupling, i.e., they capture signal similarity between smaller sets of neighboring areas, and in this sense reflect segregation mechanisms (Lioi et al., 2021). During cognitive processes, brain activity shows a strong opposing relationship between the participation of these two types of cortical gradients (Ito et al., 2020), suggesting two different types of broadcasting mechanisms underpinning functional dynamics (Park et al., 2021). In line with these ideas, we studied the dynamics of the energy distribution between the lower and higher end of the spectrum. Figs. 3A and S4A shows that the signal's power spectral distribution on the graph has a $1/\lambda$ shape. This means that most of the energy of the signal in time is concentrated in spatial patterns that are smooth (dominance of low frequencies). To investigate the broadcasting dynamics of the evoked signal, we split the graph spectrum into two parts, corresponding to the lowest and the highest end of the spectrum, following the methodology introduced in (Preti and Van De Ville, 2019) (see *Methods: Graph spectrum dichotomization*). Briefly, we computed the l_2-norm of the part of the signal belonging, to the low-frequency connectome harmonics P_L^t (and to the high-frequency connectome harmonics P_H^t, respectively) as:

$$\begin{aligned} P_L^t &= \|1_{[\lambda<\lambda_T]}\mathbf{U}^\top \mathbf{s}^t(r)_2\| \\ P_H^t &= \|1_{[\lambda\geq\lambda_T]}\mathbf{U}^\top \mathbf{s}^t(r)\|_2, \end{aligned} \tag{2}$$

where $1_{[\lambda<\lambda_T]}$ is the indicator function, which keeps only the lowest part of the spectrum (or to the highest, for $1_{[\lambda\geq\lambda_T]}$). The dynamic interplay between P_L^t and P_H^t is shown in Fig. 3B,C, (also in Fig. S4B,C for a validation in a different dataset). Fig. 3D shows a strong linear dependency between P_L^t and P_H^t and the compactness of the connectome spectrum, indicating that when compactness is maximal, brain activity is coupled over long-range network distance (integrated). In other terms, almost every time that the connectome spectrum is compact, the energy of the signal is concentrated in the low-frequency harmonics. This suggests that integration mechanisms are captured by few harmonics, whereas segregation is supported by the activation of many.

In order to summarize the broadcasting direction (BD, towards integration or segregation), for each participant and time-point we compute a single scalar value:

$$BD^t = P_H^t - P_L^t. \tag{3}$$

We tested the significance of BD against the BD estimated from degree-preserving surrogate harmonics (see *Broadcasting significance test*). The results are shown in Fig. 3D,E, and demonstrate that the broadcasting direction follows significant and consistent dynamics across time, with some variability across participants.

We refer the reader to the *Discussion* section for a detailed interpretation on the obtained dynamics of integration and segregation.

2.4. Low dimensional trajectories during visual perception

To understand how brain activity spans, or explores, a given coordinate system, it is useful to conceive of the activity as a dynamic trajectory through that space (commonly referred as state-space representation). Here, we compared activity trajectories evoked by images of faces to the trajectories evoked by images of scrambled-faces (see Fig. 4A). We represented these trajectories both in the coordinate space defined by brain regions (signal $s^t(r)$) and the coordinate space defined by connectome harmonics (signal $\hat{s}^t(\lambda)$). Scrambled-faces are a commonly used control for the influence of low-level stimulus features, given that they preserve the amount of image contrast, light intensity and spatial frequency content as in face images. The only differences expected in the estimated activity between these two stimuli are related to the face-perception mechanisms.

The trajectories in Fig. 4A show that the activation of the different dimensions over time are not completely independent in any coordinate system, i.e., they are correlated. The mean Pearson correlation among dimensions in time was 0.54 for brain areas and 0.45 for connectome harmonics ($p < .005$, Wilcoxon Rank-sum two-sided test). However, $\hat{s}^t(\lambda)$ was significantly less co-linear than the signal $s^t(r)$ (see Fig. 4B, $p < .005$, Wilcoxon Rank-sum two-sided test). These results indicate that connectome harmonics capture components of brain activity that are more spatially independent across time, and hence more likely to capture its degrees of freedom.

The degrees of freedom that encode functionally relevant features in a signal are expected to concentrate an important proportion of the signal's energy over time. For example, we can expect that a visual stimulation experiment will concentrate a great part of the brain activity signal in the occipital lobe. Here, we performed dimensionality reduction of the signal by keeping only those dimensions that concentrated most of the energy (by means of the l_2-norm) in order to estimate the quality of representation of different coordinate systems (see *Methods: Low-dimensional embedding*).

The results indicate a larger distance between the two stimulus trajectories in the low dimensional space spanned by connectome harmonics (i.e., the different stimuli are more separated). This effect is illustrated in Fig. 4C, and demonstrates that, as the dimensionality of the coordinate systems gets reduced, the brain activity trajectories evoked by faces and scrambled-faces become more separable in the connectome spectrum signal. Furthermore, the difference between these two trajectories in the reduced subspace of the connectome spectrum signal encodes a more representative brain activity map of the face-processing network (Haxby et al., 2000; Gauthier et al., 2000) (see Figs. 4D and S6). In other words, the connectome harmonics that concentrate most of the stimulus-evoked energy capture the differences between faces and scrambled-faces with higher sensitivity than the area-based analysis. These results suggest that high-level features of visual stimulus are encoded by a smaller number of connectome harmonics than brain areas. Thus, results indicate that connectome harmonics are able to capture independent neurophysiologic parameters.

Another important property of the state-space representation is that potentially functionally relevant features of the signal are encoded in the topology of the signal's trajectory (Chaudhuri et al., 2019; Rué-Queralt et al., 2021), i.e., its shape in the state-space. Accordingly, we measured for each system of coordinates how the dimensions with highest energy concentration contributed to the shape of the signal's trajectory using tools from Topological Data Analysis (Barannikov, 1994; Goodman, 2008). Specifically, we used a tool known as persistence homology of simplicial complexes, which allowed us to analyze the shape of the brain activity signal and its connectome spectrum, by means of a very simple diagram (see Fig. 5A–C). This so-called persistence diagram allowed us to analyze how the topological features were maintained

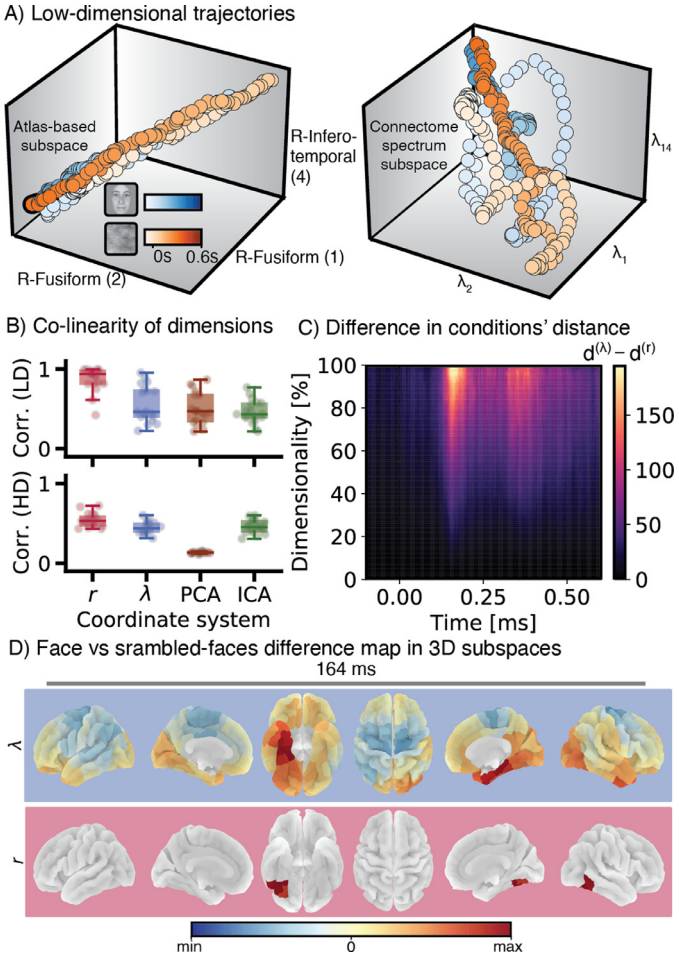

Fig. 4. Trajectories of brain activity. (A) Low-dimensional trajectories. The brain activity signal evoked by stimulation with images of faces (in blue) and scrambled-faces (in red) is represented as a vector moving in time in a three-dimensional coordinate system. The three-dimensional space is defined by those dimensions that capture more energy of the signal: (left plot) coordinate system spanned by the three top brain areas, and (right plot) coordinate system spanned by the three top connectome harmonics. (B) Co-linearity of dimensions. The co-linearity of the dimensions of each coordinate system (*r*: area-based; λ: connectome harmonics; PCA: principal components from principal component analysis; ICA: independent components from independent component analysis) is measured by the average pairwise correlation among the top three dimensions (top plot), and among all dimensions (bottom plot). (C) Difference in conditions' distance. The difference in the magnitude of the distance between brain patterns in the two different coordinate systems (regions of interest and connectome harmonics). A larger value indicates that the difference in brain activity between two conditions is larger in the subspace of connectome harmonics. A value of zero indicates that magnitude of the distance between conditions is similar in both subspaces (see *Methods: Distance between two trajectories*). (D) Face vs scrambled-faces difference map. The reconstructed pattern (for a compression percentile of 99, corresponding to keeping only the 3 dimensions shown in (A)) at the time-point in which the distance between the faces' and the scrambled-faces' trajectories is maximal in the area-based full dimensional signal (219 areas). See Fig. S6 for the participation of each brain area in the difference map compressed in the connectome spectrum (For interpretation of the references to color in this figure legend, the reader is referred to the web version of this article.).

when decreasing the number of dimensions in each coordinate system with the same criteria for reducing the dimensionality as before (dimensions were kept based on their energy concentration). In brief, the analysis of topology of brain activity signals for different dimensional state-spaces consisted of the following steps: first, the set of data points in the low-dimensional state-space (i.e., the low-dimensional signal, see

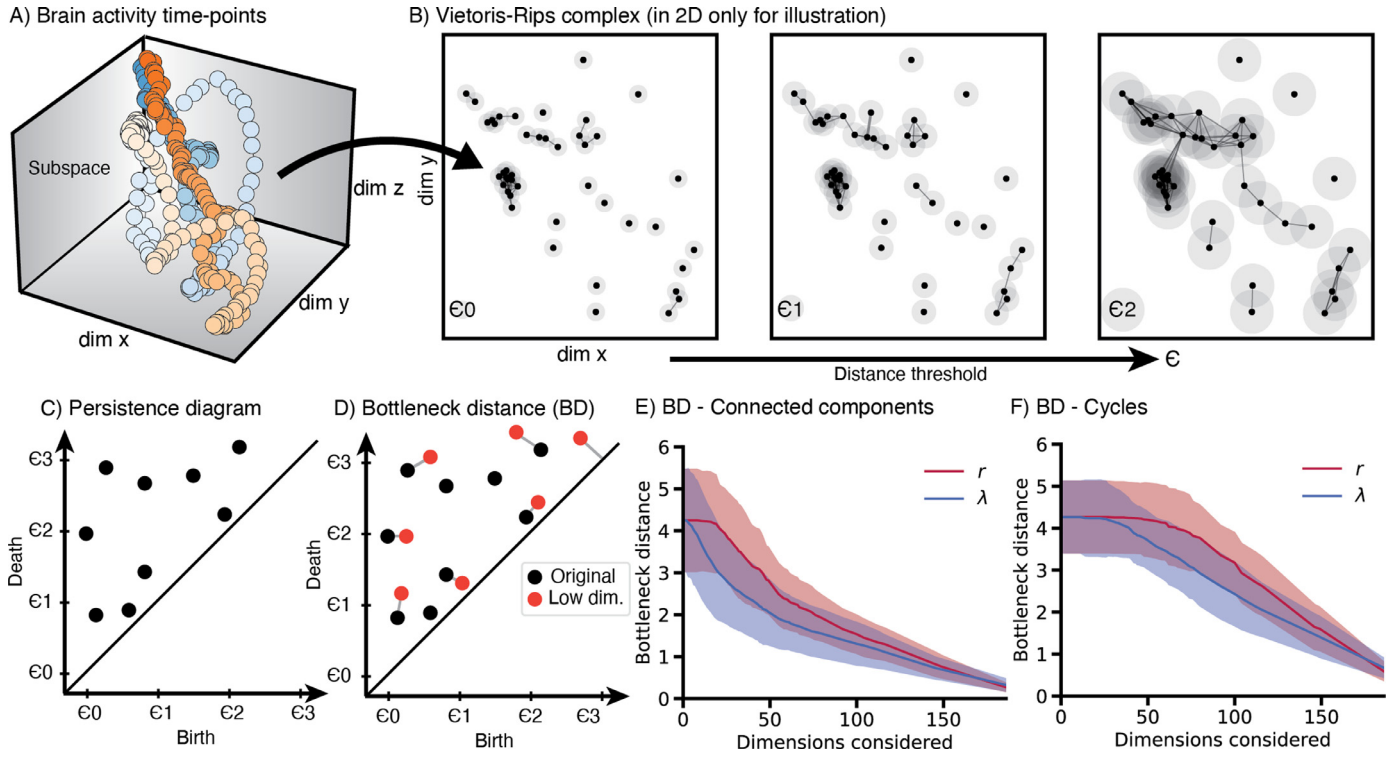

Fig. 5. Topological features of the brain activity signal in different coordinate systems. (A) Two trajectories of brain activity (corresponding to two different stimuli) are represented in a low-dimensional subspace (here $d = 3$ for illustration purposes) (B) The Vietoris-Rips Complex (VRC) is constructed from the data points in (A) (in this example, only two dimensions are shown for illustration). The VRC is generated for each trajectory individually in the following manner: for a given distance threshold ϵ, connections or edges between data points smaller than the threshold are established (see *Methods: Persistence Diagrams and Bottleneck distance*). The number of simplicial complexes (connected components and cycles) that appear (birth) or disappear (death) when increasing ϵ is registered in the persistence diagram (C). The persistence diagram summarizes the topology of the set of data points, i.e., the shape of the trajectory. (D) The distance between any two persistence diagrams can be computed with the bottleneck distance. (E)-(F) The bottleneck distance between the persistence diagrams of the original coordinate system (219 brain areas) and the reduced subspaces is shown (area-based and connectome spectrum). This distance is computed for connected components (E), and for cycles (F).

Fig. 5A) was used to generate a Vietoris-Rips complex (Hausmann, 1995) (VRC, Fig. 5B). The VRC defines the connectivity among data points based on their proximity in the state-space for a varying distance threshold ϵ. For each distance threshold ϵ, time-points are connected if they are closer than ϵ in the state-space. While varying ϵ, the appearance (birth) or disappearance (death) of new connections (topological features) is recorded in the persistence diagram (Fig. 5C). We summarized the shape of the brain activity trajectory in the two coordinate systems for any dimensionality in $[1, D]$. If a coordinate system conferred a good low-dimensional representation of the signal, i.e., if it kept the shape of the trajectory, we would expect to see that the persistence diagram of the subspace was very similar to the persistence diagram of the original high-dimensional representation. A bad low-dimensional representation would show a very different persistence diagram, as the important topological features would not be maintained. We used the bottleneck distance (Efrat et al., 2001) (see *Methods: Persistence Diagrams and Bottleneck distance*) to quantify the effect of decreasing the dimensionality of the state-space on the persistence diagram. The bottleneck distance quantifies the difference between two persistence diagrams (see Fig. 5D). The results are shown in Fig. 5E,F. When the dimensionality of the subspace was small (i.e., the dimensionality less than 50 dimensions), both the area-based signal and its connectome spectrum failed to capture the topology of the original signal. However, as the dimensionality increased, the bottleneck distance in both coordinate systems decreased, indicating that the topological features were started to be accounted for. Importantly, when comparing all the dimensions, the connectome spectrum representation better maintained, in comparison with the common brain area representation, the overall topology of the signal ($p < .001$, Wilcoxon Rank-sum two-sided test). These results show that the fast temporal dynamics of brain activity are overall better preserved in a low-dimensional subspace defined by connectome harmonics.

3. Discussion

A canonical signal representation is a representation that is the simplest or optimal in some aspect (Vault, 2021) (not to be confused with linear canonical transform (Bastiaans and Alieva, 2016)). The advantageous properties of the multi-modal connectome spectrum representation for brain activity analysis over simpler signal descriptions based on unimodal EEG data are not unexpected and have been previously proposed (Glomb et al., 2020). With the intention of rigorously benchmarking connectome spectral analysis, this work provides empirical evidence that description of neural function in terms of the functional activation of connectome harmonics has advantageous properties for the analysis of fast brain activity. When compared to the common area-based signal representation, connectome spectral analysis confers a sparser and more informative signal representation of large-scale brain activity dynamics, in the statistical, functional and topological sense.

3.1. The connectome spectrum of brain activity is sparse

With the continuous advances in neurotechnology, spatial and temporal resolution of neural activity measurements are steadily improving. When analyzing noisy high-dimensional data, transformations into sparse signal representations have two main advantages: since the degrees of freedom are low, the interpretation is tractable, and the ro-

bustness to noise is improved (Baraniuk et al., 2010). These properties make compact coordinate systems optimal to construct efficient regularizers for regression and classification models, i.e., for brain decoding. We have shown that the signal is more compressible using its connectome spectral representation than using either the original signal representation by brain areas or degree-preserving surrogate connectome harmonics (Fig. 2B). Also, this compactness is driven by the geometry of the connectome, as geometry-preserving surrogate harmonics show similar performances. This confers compelling evidence that the spatial embedding of the connectome allows the spectral decomposition of brain activity into biologically relevant parts, adding one more piece of evidence that brain activity is shaped by macroscopic structural connectivity. Furthermore, the fact that connectome spectral dimensionality reduction performs equally or better than data driven approaches (PCA and ICA) suggests that the underlying description is relevant to macroscopic brain activity, as it captures the major axes of variability in the data. Hence, the brain activity signal can be interpreted as an addition of components that define smooth variations at different scales over the structural connectivity (connectome harmonics) rather than a simple addition of the activity in individual brain regions. The plausibility of this hypothesis is strengthened by the positive linear relationship between the compactness of the connectome spectrum and the power of the signal (see Fig. 2C). To understand why this linear relationship is important, imagine any graph in which we inject a signal through one of the nodes. If the input signal has a strong power, the signal will diffuse along the whole graph following its edges, inducing a strong coupling among distant nodes that will be captured by few low-frequency harmonics, and thus it will be compact. Conversely, if the injected signal is weak, the diffusion will not reach further than the first neighbors. This later activation pattern will take the shape close to a Dirac pulse, which translates into a flat spectrum, i.e., a non-compact connectome spectral representation.

In a previous article, we have shown that the process of face perception involves the greater activation of certain structural networks over single brain areas (Glomb et al., 2020). We showed that the representation of brain signals in terms of connectome harmonics is sparse around the peak inflection of the ERP (140–340 ms post stimulus). Likewise, in Glomb et al. (2020), only a few components were needed to differentiate the brain activity pattern evoked by the two different visual stimuli. In the present study, we delve into the temporal dynamics of the signal compactness and show that compactness dynamics reflect underlying cognitive processes. We have observed different temporal regimes at which the connectome spectrum compactness is significantly higher than the compactness of the signal defined at the brain areas, and others at which they are equal. At the time of high-level face processing, at around 170 ms, the compactness of the signal is similar in both coordinate systems. This is due to the concentration of the activity into the brain regions around the FFA. As this brain activity pattern conforms a sparse signal in the area-based representation, the compactness of the signal in this coordinate system increases, and the signal spectrum compactness decreases, i.e., the signal spectrum is more broadband (equivalent to a Dirac pulse in time and its Fourier spectrum). Despite this, when compressing the signal's connectome spectrum down to just 5% of the signal, the reconstructed signal is better, in terms of correlation and reconstruction error, than the area-based compression. Importantly, Fig. S3 shows that the compactness at the connectome spectrum does not underestimate functionally relevant regions. Fig. 2E shows how the signal spectrum compression preserves much more information than the compression in the original signal domain (see also Fig. S2D for the reconstruction at two other time-points). These results can be interpreted in the light of established mechanisms of face perception, which is sustained by the activation of two concomitant pathways in the brain. The first pathway, the faster one (taking around 100 ms), is related to the processing of low-level spatial features. In this pathway, sub-cortical structures quickly activate and relay to other cortical regions, such as prefrontal areas (Johnson, 2005). This fast and integrative process, consists of large-scale coupling, and it is captured by few smooth harmonics, in a compact manner, as shown in the first significant peak in Fig. 2D. The second pathway, related to processing of higher-level features that help identifying the face, activates the ventral visual stream, peaking at 170 ms in the FFA. This coarse activation pattern is reflected by the compactness deflection around 170 ms (Kanwisher et al., 1997). After 170 ms, once the face image has been perceived, the participants engage in a decision-making process during which the brain activity seems to be dominated by large-scale, mainly frontal networks, i.e., low frequency harmonics. Then, between 300 and 600 ms after the stimulus presentation, the dynamics return to their baseline profile, dominated by higher-frequency harmonics. Given that visual networks closely match the patterns defined by low-frequency harmonics (Atasoy et al., 2016), and that a large number of harmonics of higher frequency are needed to compose networks associated with higher cognitive functions, similar results could be expected in other experiments of visual perception. We have validated this hypothesis in a visual motion detection experiment and found similar results (see Fig. S4 and Supplementary Text S1).

It is also important to take into consideration how the noise component of the signal is distributed in different coordinate systems. Before the stimulus presentation (at 0 ms), the recorded activity consists of the average brain activity across trials with very different brain states. Given that the time of the stimulus presentation is randomized, the brain signal prior to the stimulus that is averaged corresponds to the residual noise. Ideally, this noise should not be associated with any particular dimension (brain area or connectome harmonic), but it should rather be evenly distributed across dimensions. As indicated by a smaller compactness of the pre-stimulus signal in its connectome spectrum, noise co-varies less with connectome harmonics than with brain areas. In Fig. S5, we show that noise is actually not evenly spread across dimensions due to the source reconstruction bias toward smooth spatial brain activity patterns. However, this figure also shows that connectome harmonics are the most robust representation against this source-reconstruction artifact. Overall, these results suggest that the brain activity signal representation in its connectome spectrum is more noise-independent than in the traditional area-based representation.

In summary, in this section we have shown that the brain activity signal is more compact when represented as an activation of connectome harmonics, or, in other words, that the brain activity signal is sparser in its connectome spectrum.

3.2. *Broadcasting dynamics are characterized by the connectome spectral content*

Besides showing appealing statistical properties, the connectome spectrum seems to be a canonical basis for brain activity signal representation, as brain dynamics can be more efficiently described by connectome harmonics than just by isolated brain areas. In fact, the connectome spectral power density follows a λ^{-1} decay (see Fig. 3A), indicating that, overall, the signal is smooth on the graph. A smooth signal on the graph is energy efficient, and informs us that the connections that are present in the structural connectivity are also present in the functional signal (Chen et al., 2015). In this paper, we have shown that the functional connectivity dynamics can be estimated without complex models simply by measuring at each time-point the contribution of connectome harmonics (see Fig. 3B,C). We proposed a method to estimate the broadcasting profile of the brain activity signal at each time-point, characterizing brain activity in terms of integration and segregation mechanisms with respect to the underlying structural network (Tononi et al., 1994; Deco et al., 2015).

Defining functional connectivity from the connectome spectrum assumes that communication in the brain is based on a diffusion process over the structural connectivity, i.e., that brain activity propagates through the white matter. For this reason, we founded our interpretation of broadcasting dynamics upon such a communication model. The interpretation of brain function as a combination of con-

nectome harmonics has recently been receiving an increasing support (Haak and Beckmann, 2020), and it reflects how the brain function is organized hierarchically (Betzel and Bassett, 2017).

We have been inspired by the fact that functional integration and segregation are strongly related to connectome harmonics (Wang et al., 2019), with low-frequency harmonics being associated with integration and higher-frequency harmonics being associated with segregation mechanisms. When applied to visual evoked potentials in a face perception experiment (and in a motion perception experiment in the supplementary material), the broadcasting analysis revealed that integration and segregation follow significant and consistent fast dynamics across all participants, and are closely related to the compactness of the signal in its connectome spectrum (see Fig. 3D,E). During high-frequency visual processes, such as the integration of visual features into a whole object, or the decision-making process that follows, the brain activity signal is dominated by low-frequency harmonics that capture large-scale connectivity. During that period, the brain is in an integrated configuration, and there is an increase in the signal compactness. Conversely, during segregated processing, i.e., the initial parallel processing of low-level features, or the peak activation of specialized FFA during face perception, high-frequency harmonic components redistribute and collectively reduce the signal compactness.

3.3. The structure of the brain shapes its dynamics

So far, we have shown that connectome spectral decomposition not only provides us with a robust and sparse representation for brain activity, but also enables the natural description of the broadcasting profile of the signal, indicating whether the brain state is in an integration or a segregation mode. These can be regarded as some general properties of the signals defined on the graph. We wanted to evaluate whether connectome spectral analysis can show any added value to the study of brain activity dynamics.

It is common in theoretical neuroscience to represent the dynamics of brain activity as a trajectory in its state-space, i.e., as a point that moves in time in the space defined by the activity of each neuron or neural population (Hopfield, 1982) (see Figs. 4A and 5A). In this context, the working hypothesis is that high-level neural computation in the brain involves the formation of low-dimensional temporal structures in the state-space. These low-dimensional structures are known as attractors (Seung, 1996; Burak and Fiete, 2009). In this work, we have studied how the brain activity evoked by visual stimuli formed low-dimensional structures spanned by either brain areas or by connectome harmonics.

Our results show that functionally relevant properties of the signal are characterized with more sensitivity when the state-space is defined by the signal's connectome spectrum, rather than by the activity of isolated brain areas. More specifically, we have characterized two different properties of the signal.

On the one hand, we have shown that the brain activity spatial maps captured by the connectome spectrum are more independent in time (Fig. 4B). It is probably due to this fact that the distance between the trajectories corresponding to brain activity processing of two different types of information (low-level vs. high-level visual stimuli features) is higher in the subspace of the connectome spectrum (Fig. 4C). Not only the two types of stimuli are more separable in the connectome spectrum, but connectome harmonics also represent more accurately the complex networks underlying the physiological mechanisms (Fig. 4D).

On the other hand, we have investigated another important property of the state-space: its contribution to the shape of the brain activity temporal structure (Chaudhuri et al., 2019). It has been proposed that human whole-brain dynamics lie onto a low-dimensional manifold, whose shape is directly related to behavior (Saggar et al., 2018; Shine et al., 2019; Rué-Queralt et al., 2021). Using topological data analysis (Barannikov, 1994; Goodman, 2008), we have quantified the contribution of each coordinate system's state-space to the overall shape of the brain activity trajectory (Fig. 5A,B). The results of this last analysis indicated that the effect of reducing the state-space dimensionality has a more negative impact on the shape of the trajectories for the area-based representation. In other words, that connectome spectrum representation of the signal captures the important features of the brain activity dynamics with a smaller number of dimensions.

3.4. Limitations and future directions

There are some important limitations in our study. The most important of them is associated with the use of EEG data. The spatial smoothness of the inverse solution used could bias the estimated coupling between structure and function. This limitation is made obvious by the fact that there is one type of connectome spectrum configuration that we have not observed in our data: the activation of single, or very few high-frequency harmonics during the visual evoked activity (see Fig. 1F). In our datasets, these components activate very weakly. The relatively smooth nature of the reconstructed electrical activity implies that very high-frequency connectome harmonics will always have small weight in the signal. However, the smoothness of the source reconstruction does not completely account for the prominence of the low-frequency components, which are spatially much smoother (see Fig. S1). For the analysis of compactness, we have tested the effect of such bias with simulations, and observed that the connectome spectrum is the most robust representation to this artifact (see Fig. S5). fMRI research has already shown that connectome harmonics capture the main axes of the variability of the spatiotemporal dynamics, as their composition conform the different resting-state networks (Atasoy et al., 2016), and their dynamics are altered by drugs in a harmonic-selective manner (Atasoy et al., 2017). For this reason, we believe that the connectome spectrum would also form a sparse and lower-dimensional basis for fMRI data, and propose its study for future research.

Regarding the analysis of integration and segregation, we compensate for the source-reconstruction smoothing bias towards low-frequency harmonics by defining integration and segregation in a data-driven manner. More specifically, we define a threshold that divides the connectome spectrum energy across all time into two halves (which may be composed of a different number of harmonics). If instead, we chose to divide the connectome spectrum into two halves with the same number of harmonics, most of the energy would be concentrated in the lowest end of the spectrum (smooth harmonics), and the system would be always defined as integrated. However, the effect of the source reconstruction strategy and accuracy on our results should be addressed in future studies.

A related limitation is the general difficulty of the Fourier transform to pick up transients in the graph, such as a Dirac delta function, in a compact manner. This is the same in the case of spatial and temporal Fourier analysis. Such transient patterns are better captured by the signal representation based on brain areas (which are Dirac delta functions). A possible solution to be investigated in future work could be the use of graph wavelets (Hammond et al., 2011) instead of connectome harmonics, as they excel at picking up transient signals in a compact manner.

Our results suggest that the shape of the structural connectivity plays a very important role in the signal decomposition. Interesting future directions could be to study how the inter-individual variability on the structural connectivity modulates the spectral representation of the signal. This approach would be very challenging, given that different graph-structures would provide different connectome harmonics, and the comparison between participants would not be straight forward. Similarly, future directions could point towards hallmarks of brain disorders in which the structural connectivity is affected.

Taking into account that connectome spectral analysis assumes brain activity as a diffusion process on top of the structural connectivity, the fact that geometry-preserving harmonics provided a similar compactness performance than the connectome harmonics suggests that connectome weight model (number of fibers) that we used might not be

the most accurate model to capture the diffusion dynamics of the brain. However, the fact that geometry-preserving surrogates perform better than degree-preserving surrogates suggests that the spatial embedding of the connectome is a property more important than the weight model to describe brain dynamics compactly. For future work, an interesting perspective is to study compactness analysis as a cost function to optimize the weight-model selection for connectomics.

Another important aspect to take into consideration, is that the functional connectivity measures (integration and segregation) estimated in this work are parametric, i.e., they assume that brain activity diffuses over the structural connectivity graph. For this reason, it is crucial that when interpreting those measures, one considers that they ultimately depend on the validity of the underlying communication model (Seguin et al., 2020).

A potential different line of research to follow-up on this work would be the study of the time-vertex joint power-spectral density (see Grassi et al. 2017). In that direction, the joint signal representation of spatial and temporal modes could be related to the theories of communication through coherence (Fries, 2015) and brain oscillations (Raj et al., 2020). In this sense, it would be very interesting to investigate the role of the connectivity measures used to define the edges in the structural connectivity matrix. Here we used the number of fibers connecting every pair of brain areas (estimated from tractography). The connectome harmonics would have been different if we used the average fiber length instead. This last approach could be useful to investigate the role of delays in functional connectivity.

Finally, further validation is needed in different contexts, to verify whether the conclusions and hypotheses presented hold for a larger variety of tasks.

4. Materials and methods

4.1. Data acquisition and pre-processing

High-density EEG was recorded at 2048 Hz using a 128-channel Biosemi Active Two EEG system (Biosemi, Amsterdam, The Netherlands;) at the Fribourg Cantonal Hospital, Fribourg, Switzerland. A total of 20 healthy participants (17 females, mean age: 23, age range: 20–29 years) were recorded while performing a visual discrimination task. All participants provided written informed consent before the experiment. The experimental procedures complied with the Declaration of Helsinki and were approved by the regional ethics board (CER-VD, Protocol Nr. 2016–00,060). A good signal quality was guaranteed by keeping the offset between the active electrodes and the Common Mode Sense - Driven Right Leg (CMS-DRL) feedback loop under a standard value of ±20 mV. After each participant session, individual 3D electrode positions were digitized with an ultrasound motion capture system (Zebris Medical GmbH). This open dataset (Pascucci et al., 2021) has been used in previous publications (Glomb et al., 2020; Rubega et al., 2019). The visual stimuli consisted of images of faces or scrambled versions of the same images (Ales et al., 2012). After a 200 ms image presentation, participants responded by pressing one of two buttons on a response box, whether they had seen a face or a scrambled image. One participant was excluded due to motion artifacts, leaving 19 datasets for analysis. Data were pre-processed using EEGLAB v14.1.1 (Delorme and Makeig, 2004) (*sccn.ucsd.edu/eeglab/index.php*). Downsampling to 250 Hz (anti-aliasing filter: cut-off frequency of 112.5 Hz; transition bandwidth of 50 Hz) and local detrending (high-pass filter at 1 Hz, EEGLAB PREP plugin) were applied (Bigdely-Shamlo et al., 2015). Trials were extracted from 1500 ms before the stimulus presentation until 1000 ms after. Line and monitor noise (at 50 and 75 Hz, respectively, as well as harmonics of these frequencies) were removed by spectral interpolation (Leske and Dalal, 2019). Bad trials (22 ± 36 out of 600 per participant) were removed and bad channels (15 ± 9 out of 128 per participant) marked via visual inspection. The remaining physiological artifacts (eye blinks, horizontal and vertical eye movements, muscle potentials) were removed using FastICA by first marking bad ICs using the Multiple Artifact Rejection Algorithm (MARA) as implemented in EEGLAB (Delorme and Makeig, 2004). The previously identified bad channels were not included in this step. Finally, bad channels were interpolated using the nearest neighbor spline method as implemented in EEGLAB, and data were re-referenced to the common average before being globally z-scored.

4.2. Structural MRI

T1-weighted images were obtained from the same participants as magnetization prepared rapid-gradient echo (MPRAGE) volumes using a General Electrics Discovery MR750 3T MRI scanner and a COR FSPGR BRAVO pulse sequence with flip angle = 9°; echo time = 2.81 ms, repetition time = 7.27 ms, inversion time = 0.9 s, slice thickness = 1 mm, head first supine. Connectome mapper 3 (Tourbier et al., 2020) v3.0.0-RC1 with Freesurfer 6.0.1 were used to perform the segmentation of the MPRAGE volume into gray and white matter, as well as the parcellation of gray matter brain regions of interest according to the Lausanne 2008 multiscale parcellation (Hagmann et al., 2008). Connectome Mapper 3 and Freesurfer are available at *github.com/connectomicslab/connectomemapper3* and *surfer.nmr.mgh.harvard.edu/fswiki/FreeSurferWiki*.

4.3. Diffusion MRI

To create the structural connectivity matrix, we obtained a consensus connectome from an online available dataset consisting of 70 healthy participants (Griffa et al., 2019) available at *zenodo.org/record/2,872,624*; mean age 29.7 years, range 18.5–59.2 years; 34 females), scanned in a 3-Tesla MRI scanner (Trio, Siemens Medical, Germany) with a 32-channel head-coil. Informed written consent in accordance with institutional guidelines (protocol approved by the Ethics Committee of Clinical Research of the Faculty of Biology and Medicine, University of Lausanne, Switzerland, #82/14, #382/11, #26.4.2005) was obtained for all subjects. A diffusion spectrum imaging (DSI) sequence (128 diffusion-weighted volumes and a single b0 vol, maximum b-value 8000 s/mm2, 2.2 × 2.2 × 3.0 mm voxel size) was applied, and DSI data were reconstructed following the protocol described in (Wedeen et al., 2008). A magnetization-prepared rapid acquisition gradient echo (MPRAGE) sequence sensitive to white/gray matter contrast (1 mm in-plane resolution, 1.2 mm slice thickness) was also applied, and gray and white matter were segmented from the MPRAGE volume using Freesurfer and Connectome Mapper 3 (Tourbier et al., 2020).

Then, individual structural connectivity matrices were estimated by deterministic streamline tractography on the reconstructed DSI data, by seeding 32 streamlines per diffusion direction in each white matter voxel (Wedeen et al., 2008). The number of fibers found between each voxel at the gray matter/white matter-interface was summed within each brain area given by the same parcellation used for the structural data.

A consensus group-representative structural brain connectivity matrix was generated from the connectomes of 70 healthy participants using the method introduced in (Betzel et al., 2019). This method selects a recurrence threshold that is distance-dependent, and preserves the connection density across different levels of connection fiber-length. The connection density is preserved independently for intra- and interhemispheric connections, allowing more inter-hemispheric connections to be kept in the group estimate, in comparison to simple connectome average across subjects. The resulting connection density in the group connectome results in approximately 13%. The code to generate this consensus connectome is openly available at https://www.brainnetworkslab.com/s/distanceDependent.zip.

4.4. Source reconstruction and area-based time-courses

Gray matter (source) signal reconstruction of the scalp EEG signals was performed using individual realistic head conductor models, based on the tissue segmentation of the individual structural images and the EEG electrode positions. Both forward solutions, using the Locally Spherical Model with Anatomical Constraints (LSMAC) and inverse solutions, using the Local Autoregressive Average (LAURA) method, were implemented with the CARTOOL toolbox (Brunet et al., 2011) (freely available at https://sites.google.com/site/cartoolcommunity/).

Using the inverse solution matrix, we projected the EEG data of each participant into approximately 5000 dipole locations uniformly distributed in the gray matter. Apart from a magnitude, each dipole has a three-dimensional orientation. The time-series for each brain area was extracted from dipoles whose location overlapped with that region. Using the singular value decomposition method (Rubega et al., 2019), we estimated the orientation of maximal variance during the time window defined from 120 to 500 ms after stimulus onset. Each dipole in the brain area was then projected to the estimated orientation, and the average magnitude of the projection across dipoles was taken as the brain area value for each time-point.

4.5. Graph signal processing

4.5.1. Connectome harmonics and graph Fourier transform

The connectome harmonics are the eigenfunctions of the structural connectivity graph Laplacian. Given a structural connectivity graph $\mathcal{G}(D, E)$ of D nodes and E edges, we define the graph Laplacian as:

$$\mathcal{L}_{\mathcal{G}} = D - W, \tag{4}$$

where $\mathbf{D}$ is the degree matrix and $\mathbf{W}$ is the weight matrix. Here we used the normalized graph Laplacian, which is defined as:

$$L = \mathbf{D}^{-\frac{1}{2}} \mathcal{L}_{\mathcal{G}} \mathbf{D}^{-\frac{1}{2}}. \tag{5}$$

The connectome harmonics are obtained by the eigendecomposition of the normalized graph Laplacian:

$$L = U \Lambda \mathbf{U}^{\top}, \tag{6}$$

where $[\Lambda]_{dd} = \lambda_d$ for $n = [1, \ldots, D]$ are the eigenvalues of the graph Laplacian ordered according to smoothness, and are associated with the d-th eigenvector (connectome harmonic) contained in the d-th column of U. We formulate the graph Fourier transform (GFT$\{\mathbf{s}_r^t\}$) of the brain activity defined in the area-based coordinate system at a given moment in time ($\mathbf{s}_r^t \in \mathrm{R}^D$) as following:

$$\hat{\mathbf{s}}_{\lambda}^t = GFT\left\{\mathbf{s}_r^t\right\} = \mathbf{U}^{\top}\mathbf{s}_r^t. \tag{7}$$

The GFT linearly maps the original signal into the connectome harmonics. To project back the signal to the area-based coordinate system, we define the inverse graph Fourier transform iGFT as:

$$\mathbf{s}_r^t = iGFT\left\{\hat{\mathbf{s}}_{\lambda}^t\right\} = U\hat{\mathbf{s}}_{\lambda}^t. \tag{8}$$

These operations were implemented using the Graph Signal Processing toolbox in Python available at https://pygsp.readthedocs.io/en/stable/.

4.5.2. Graph power spectral density

The graph power spectral density describes the amount of energy present in each connectome harmonic during a graph time-varying signal. We compute the normalized graph power spectral density for each participant by: first transforming the evoked signal (i.e., the average signal across trials) into its connectome spectrum through the GFT. Then normalizing the connectome spectrum of the evoked signal by the standard deviation in time. Finally, the power is defined as the mean squared signal's spectrum across time.

4.5.3. Graph spectrum dichotomization

Graph spectrum dichotomization was first introduced in Preti and Van De Ville (2019). First, we decompose the brain activity signal in low-frequency and high-frequency connectome harmonic parts. These two signals are computed by multiplying the graph Fourier transformed coefficients by the indicator function to the first T lowest eigenvalues and to the $D - T$ highest eigenvalues, where λ_T is the threshold graph-frequency that divides the graph energy spectrum in two halves:

$$\begin{aligned} \mathbf{P}_L^t &= \left\| 1_{[\lambda<\lambda_T]} \mathbf{U}^{\top}\mathbf{s}^t(r)_2 \right\| \\ \mathbf{P}_H^t &= \left\| 1_{[\lambda\geq\lambda_T]} \mathbf{U}^{\top}\mathbf{s}^t(r)_2 \right\|, \end{aligned} \tag{9}$$

where $1_{[\lambda<\lambda_T]}$ is the indicator function, which keeps only the lowest part of the spectrum (or to the highest, for $1_{[\lambda\geq\lambda_T]}$). These power time-courses inform about the amount of energy of the original signal contained in the lowest- and highest-end of the graph spectrum for each time-point.

4.5.4. Surrogate harmonics

A thousand surrogate connectome graphs were obtained using the Brain Connectivity Toolbox (Rubinov and Sporns, 2010) function *null_model_und_sign*. This function shuffles the connections of the original connectome while preserving its degree distribution. The harmonics from these surrogate graphs are referred to as degree-preserving surrogate harmonics.

Another thousand surrogate connectome graphs were obtained using the "Geometry Surrogate Networks" code from http://www.sng.org.au/Downloads. This function shuffles the connection weights of the original connectome while preserving its connectivity structure. The harmonics from these surrogate graphs are referred to as geometry-preserving surrogate harmonics.

4.6. Analysis of compactness

4.6.1. Signal compactness in a given coordinate system

Signal compactness was measured using two metrics: The Person correlation between the original and the compressed signal, and the compression reconstruction error. These two metrics are based on first compressing the signal using:

$$\hat{\mathbf{X}}_i^{(p)} = \begin{cases} \mathbf{X}_i & \text{if } \left\|\mathbf{X}_i\right\|_{\mathrm{F}} \geq \mathrm{f}\left(\mathbf{X}, \|\cdot\|_{\mathrm{F}}, p\right) \\ 0 & \text{otherwise} \end{cases}, \tag{10}$$

for $\mathbf{X} \in \mathrm{R}^{D,T,N}$ and $\mathbf{X}_i \in \mathrm{R}^{T,N}$ corresponding to the T samples and N trials of the i-th dimension out of D total dimensions (brain areas or harmonics), where $\|\cdot\|_{\mathrm{F}}$ is the Frobenius norm. $\mathrm{f}()$ is a function that returns the value of the p-th percentile in the distribution of the norms of all dimensions. This compression removes the dimensions with the smallest amount of signal power throughout time and trials.

Given a signal $\mathbf{X}^{(\mathrm{S})} \in \mathrm{R}^{D,T,N}$, D the dimensionality, T the number of samples, and N the number of trials, and $\hat{\mathbf{X}}^{(S)^{(p)}}$ the compressed signal, the reconstruction normalized mean squared error (or just reconstruction error) for a given percentile is computed as:

$$c^{(\mathrm{p})} = \frac{\left\|\langle \mathbf{X}^{(\mathrm{S})} \rangle\right\|_{\mathrm{F}} - \left\|\left\langle \hat{\mathbf{X}}^{(S)^{(p)}} \right\rangle - \langle \mathbf{X}^{(\mathrm{S})} \rangle\right\|_{\mathrm{F}}}{\left\|\langle \mathbf{X}^{(\mathrm{S})} \rangle\right\|_{\mathrm{F}}}, \tag{11}$$

where $\langle\cdot\rangle$ denotes the average across trials. Compression correlation is defined as:

$$r^{(p)} = \rho\left(\left\langle \mathbf{X}^{(\mathrm{S})},\ \hat{\mathbf{X}}^{(S)^{(p)}} \right\rangle\right). \tag{12}$$

When computing compactness dynamics, we first define compression as:

$$\hat{\mathbf{X}}_{i,t}^{(p)} = \begin{cases} \mathbf{X}_{i,t} & \text{if } \left\|\mathbf{X}_{i,t}\right\|_2 \geq \mathrm{f}\left(\mathbf{X}_{:t}, \|\cdot\|_2, p\right) \\ 0 & \text{otherwise} \end{cases}, \tag{13}$$

for $\mathbf{X}_{i,t} \in \mathrm{R}^N$ corresponding to the N trials of the i-th dimension at sample t of $\mathbf{X}$, where $\|\cdot\|_2$ is the l_2-norm. $\mathrm{f}()$ is a function that returns the

value of the p-th percentile in the distribution of the norms of all dimensions. We then define compactness dynamics (c_t) as the average reconstruction performance (1 − reconstruction error) of the compressed signal across all percentiles at each time-point:

$$c_t = \frac{1}{100}\sum_{p=1}^{100}\frac{\|\langle \mathbf{X}_{:t}\rangle\|_2 - \left\|\left\|\hat{\mathbf{X}}_{:t}^{(p)}\right\| - \langle \mathbf{X}_{:t}\rangle\right\|_2}{\|\langle \mathbf{X}_{:t}\rangle\|_2}, \tag{14}$$

where $\langle \mathbf{X}_{:t}\rangle \in \mathrm{R}^D$ (and$\langle \hat{\mathbf{X}}_{:t}^{(p)}\rangle \in \mathrm{R}^D$) is the average pattern (across trials) of the original signal (compressed signal at a given percentile) across all trials at time t. Please note the differences when measuring compactness in Eq. (11).

4.6.2. Compression effect on visual streams

We assessed whether the effect of compressing the signal was harmful at specific brain areas known to be involved in visual processing. For that reason, we defined the dorsal and ventral streams, and a group of early visual areas, by clustering some of the 219 regions of interest in scale 3 of the multi-scale Lausanne atlas parcellation (Cammoun et al., 2012). The choice of brain areas used is shown in Fig. S3, and was based on a previous study finding clusters corresponding to the different visual pathways (see Fig. S4 in the Ref. Hagmann et al. 2008). Compactness metrics were computed only taking into account the signal in those areas. To do so, in the case of the connectome spectrum, the signal of brain region activity was uncompressed using a set of coefficients estimated by compression, by means of the iGFT defined in Eq. (8).

4.6.3. Conditional probabilities

The conditional probability of the compactness of the evoked signal $\langle \mathbf{X}^{(\mathrm{S})}\rangle \in \mathrm{R}^{D,T}$ in a given coordinate system S, given the signal power was computed as the following. First, we computed the compactness dynamics, using Eq. (12). We then removed the outliers (3 standard deviations) and computed the joint probability of signal compactness and power:

$$P\left(c_t^S, \left\|\mathbf{X}^{(\mathrm{S})}\right\|_2\right), \tag{15}$$

using the Gaussian kernel density estimation from the python SciPy toolbox (Virtanen et al., 2020). From the joint probability, we obtained the marginal probability of the signal power. The conditional probability was finally obtained as:

$$P\left(c_t^S \middle| \left\|\mathbf{x}^{(S)}\right\|\right) = \frac{P\left(c_t^S, \left\|\mathbf{x}^{(\mathrm{S})}\right\|_2\right)}{P(\|\mathbf{x}^{(\mathrm{S})}\|_2)}. \tag{16}$$

4.7. Statistical analysis

4.7.1. Difference in compactness dynamics between different coordinate systems

The significance of the difference in compactness dynamics between two coordinate systems was assessed by means of Monte-Carlo simulations. Specifically, we designed a permutation test to generate a null model distribution of "no difference of compactness between coordinate systems". This null model was generated by computing n_{perm}-times the difference between two matrices that were randomly sampled from the compactness matrices of the two coordinate systems. For each permutation, these two matrices contained the data from half of the subjects in one coordinate space, and half of the subjects in the other. n_{perm} was computed taking into account a significance level of $\alpha = 0.05$, and the number of comparisons to be corrected for by the Bonferroni method, as follows:

$$n_{perm} = \frac{50\ n_{comp}}{\alpha} \tag{17}$$

Finally, a compactness difference was considered significant, if the empirical difference was among the 5% of the extremes of the null model distribution. For this purpose, the Bonferroni corrected p-value was computed for each time-point as:

$$p(t) = n_{comp}\frac{\sum_i^{n_{perm}} f\left(\mathrm{diff}(t), \mathrm{diff}_{perm}^i(t)\right) + 1}{n_{perm} + 1}, \tag{18}$$

where

$$f\left(\mathrm{diff}, \mathrm{diff}_{perm}^i\right) = \begin{cases} 1, & diff < \mathrm{diff}_{perm}^i, \\ 0, & diff \geq \mathrm{diff}_{perm}^i. \end{cases} \tag{19}$$

4.7.2. Broadcasting significance test

The significance of the broadcasting dynamics was assessed by a statistical test based on comparing against the broadcasting dynamics described by surrogate networks. More specifically, we first obtained a single scalar summary of the broadcasting dynamics for each subject and time-point, namely the broadcasting direction (BD):

$$\mathrm{BD}^t = \mathbf{P}_H^t - \mathbf{P}_L^t \tag{20}$$

We then computed the BD for the degree-preserving surrogate harmonics (see *Surrogate harmonics*) and created a null distribution. For each time-point and subject, a p-value was computed following the same approach as in the previous section *Difference in compactness dynamics between different coordinate systems*. However, due to the increase in the number of comparisons (as we tested for each subject separately), we corrected for multiple comparisons with the Benjamini Hochberg FDR method from the Python toolbox https://www.statsmodels.org/.

4.8. Dimensionality analysis

4.8.1. Co-linearity of dimensions

Co-linearity of dimensions was measured by first computing the correlation matrices:

$$R_{i,j} = \rho\left(\mathrm{vec}\left(\mathbf{X}_i^{(\mathrm{S})}\right), \mathrm{vec}\left(\mathbf{X}_j^{(\mathrm{S})}\right)\right), \tag{21}$$

where $\mathbf{X}_i^{(\mathrm{S})} \in \mathrm{R}^{T,N}$ corresponds to the data in the i-th dimension of the coordinate system S, with T samples and N trials, and after vectorization $\mathrm{vec}(\mathbf{X}_i^{(\mathrm{S})}) \in \mathrm{R}^{TN}$.

4.8.2. Distance difference between different trajectories

We computed the distance between two trajectories of brain activity for each time-point as:

$$d^{(\mathrm{S})}(t) = \left\|\left\langle \hat{\mathbf{X}}_{:t}^{(\mathrm{S},i)}\right\rangle - \left\langle \hat{\mathbf{X}}_{:t}^{(\mathrm{S},j)}\right\rangle\right\|, \tag{22}$$

where $\hat{\mathbf{X}}_{:t}^{(\mathrm{S},k)} \in \mathrm{R}^d$ is the average brain activity pattern across the many trials corresponding to the k-th condition (faces vs scrambled) at time t, in the coordinate space S (area-based vs connectome harmonics).

We then defined the difference between the distances estimated at different coordinate-systems' sub-spaces as:

$$d(t,p) = d^{(\mathrm{S}_1,\mathrm{p})}(t) - d^{(\mathrm{S}_2,p)}(t), \tag{23}$$

where (S_1, p) indicates that distance is computed for the subspace of the coordinate system S_1 defined by the percentile p (see *Low-dimensional embedding*).

4.8.3. Low-dimensional embedding

We followed the dimensionality reduction approach based on the same criterion as the compression in Eq. (10). Namely, to reduce the dimension to a given percentile p we keep the i-th dimension if:

$$\|\mathbf{X}_i\|_{\mathrm{F}} \geq \mathrm{f}\left(\mathbf{X}, \|\cdot\|_{\mathrm{F}}, p\right), \tag{24}$$

for $\mathbf{X}_{i,t} \in \mathrm{R}^N$ corresponding to the N trials of the i-th dimension at sample t of $\mathbf{X}$, where $\|\cdot\|_{\mathrm{F}}$ is the Frobenius norm. $\mathrm{f}()$ is a function that returns the value of the p-th percentile in the distribution of the norms of all dimensions.

4.8.4. Persistence diagrams and bottleneck distance

To compute the persistence diagrams of the trajectories, we used the package Ghudi available at http://gudhi.gforge.inria.fr. Persistence diagrams were generated for connected components and cycles, for coordinate systems with a varying number of dimensions, using the low-dimensional embedding explained above. Then we computed the bottleneck distance between the persistence diagrams of the original signal (219 areas) and the persistence diagram of the signal in the subspace of the different dimensions.

Declaration of Competing Interest

All other authors declare they have no competing interests.

Credit authorship contribution statement

Joan Rué-Queralt: Conceptualization, Data curation, Investigation, Visualization, Writing – original draft, Writing – review & editing. **Katharina Glomb:** Conceptualization, Investigation, Writing – review & editing. **David Pascucci:** Data curation, Investigation, Writing – review & editing. **Sébastien Tourbier:** Data curation, Writing – review & editing. **Margherita Carboni:** Data curation, Writing – review & editing. **Serge Vulliémoz:** Supervision, Writing – review & editing. **Gijs Plomp:** Conceptualization, Investigation, Supervision, Writing – original draft, Writing – review & editing. **Patric Hagmann:** Conceptualization, Investigation, Supervision, Writing – original draft, Writing – review & editing.

Acknowledgments

None.

Funding

This work was supported by:
Swiss National Science Foundation Sinergia Grant 170873 (PH)
Swiss National Science Foundation Sinergia Grant 192749 (SV)
Swiss National Science Foundation Sinergia Grant PP00P1_183714 (GP)
Swiss National Science Foundation Sinergia Grant PP00P1_190065 (GP)
Swiss National Science Foundation Sinergia Grant PZ00P1_179988 (DP)

Data and materials availability

Links to all data are available in the part of the text describing them. All the code used can be found at https://github.com/joanrue/connectome_spectral_analysis.

Supplementary materials

Supplementary material associated with this article can be found, in the online version, at doi:10.1016/j.neuroimage.2021.118611.

References

Abdelnour, F., Dayan, M., Devinsky, O., Thesen, T., Raj, A., 2018. Functional brain connectivity is predictable from anatomic network's Laplacian eigen-structure. Neuroimage 172, 728–739.
Ales, J.M., Farzin, F., Rossion, B., Norcia, A.M., 2012. An objective method for measuring face detection thresholds using the sweep steady-state visual evoked response. J. Vis. 12 (10), 18 –18.
Atasoy, S., Donnelly, I., Pearson, J., 2016. Human brain networks function in connectome-specific harmonic waves. Nat. Commun. 7, 10340.
Atasoy, S., Roseman, L., Kaelen, M., Kringelbach, M.L., Deco, G., Carhart-Harris, R.L., 2017. Connectome-harmonic decomposition of human brain activity reveals dynamical repertoire re-organization under LSD. Sci. Rep. 7 (1), 17661 Dec.
Avena-Koenigsberger, A., Misic, B., Sporns, O., 2018. Communication dynamics in complex brain networks. Nat. Rev. Neurosci. 19 (1), 17–33 Jan.
Baraniuk, R.G., Candes, E., Elad, M., Ma, Y., 2010. Applications of sparse representation and compressive sensing [scanning the issue]. Proc. IEEE 98 (6), 906–909.
Barannikov, S., 1994. The framed morse complex and its invariants. Am. Math. Soc. Transl. 2, 21.
Bastiaans, M.J., Alieva, T., 2016. The linear canonical transformation: definition and properties. In: Linear Canonical Transforms. Springer, pp. 29–80.
Belkin, M., Niyogi, P., 2001. Laplacian eigenmaps and spectral techniques for embedding and clustering. Nips 14 (14), 585–591.
Bentin, S., Allison, T., Puce, A., Perez, E., McCarthy, G., 1996. Electrophysiological studies of face perception in humans. J. Cogn. Neurosci. 8 (6), 551–565.
Betzel, R.F., Bassett, D.S., 2017. Multi-scale brain networks. Neuroimage 160, 73–83 Oct.
Betzel, R.F., Griffa, A., Hagmann, P., Mišić, B., 2019. Distance-dependent consensus thresholds for generating group-representative structural brain networks. Netw. Neurosci. 3 (2), 475–496.
Bigdely-Shamlo, N., Mullen, T., Kothe, C., Su, K.-.M., Robbins, K.A., 2015. The PREP pipeline: standardized preprocessing for large-scale EEG analysis. Front. Neuroinform. 9, 16.
Brunet, D., Murray, M.M., Michel, C.M., 2011. Spatiotemporal analysis of multichannel EEG: CARTOOL. Comput. Intell. Neurosci. 2011.
Burak, Y., Fiete, I.R, 2009. Accurate lompath integration in continuous attractor network models of grid cells. PLoS Comput. Biol. 5 (2), e1000291.
Cammoun, L., Gigandet, X., Meskaldji, D., Thiran, J.P., Sporns, O., Do, K.Q., et al., 2012. Mapping the human connectome at multiple scales with diffusion spectrum MRI. J. Neurosci. Methods 203 (2), 386–397.
Candes, E.J., Davenport, M.A., 2013. How well can we estimate a sparse vector? Appl. Comput. Harmon. Anal. 34 (2), 317–323.
Chaudhuri, R., Gerçek, B., Pandey, B., Peyrache, A., Fiete, I., 2019. The intrinsic attractor manifold and population dynamics of a canonical cognitive circuit across waking and sleep. Nat. Neurosci. 22 (9), 1512–1520 Sep.
Chen, S., Varma, R., Singh, A., Kovačević, J., 2015. Signal representations on graphs: tools and applications. arXiv preprint arXiv:151205406.
Deco, G., Jirsa, V.K., Robinson, P.A., Breakspear, M., Friston, K., 2008. The dynamic brain: from spiking neurons to neural masses and cortical fields. PLoS Comput. Biol. 4 (8).
Deco, G., Tononi, G., Boly, M., Kringelbach, M.L., 2015. Rethinking segregation and integration: contributions of whole-brain modeling. Nat. Rev. Neurosci. 16 (7), 430–439.
Delorme, A., Makeig, S., 2004. EEGLAB: an open source toolbox for analysis of single-trial EEG dynamics including independent component analysis. J. Neurosci. Methods 134 (1), 9–21.
Desikan, R.S., Ségonne, F., Fischl, B., Quinn, B.T., Dickerson, B.C., Blacker, D., et al., 2006. An automated labeling system for subdividing the human cerebral cortex on MRI scans into gyral based regions of interest. Neuroimage 31 (3), 968–980.
Efrat, A., Itai, A., Katz, M.J., 2001. Geometry helps in bottleneck matching and related problems. Algorithmica 31 (1), 1–28.
Fan, L., Li, H., Zhuo, J., Zhang, Y., Wang, J., Chen, L., et al., 2016. The human brainnetome atlas: a new brain atlas based on connectional architecture. Cereb. Cortex 26 (8), 3508–3526.
Fries, P., 2015. Rhythms for cognition: communication through coherence. Neuron 88 (1), 220–235.
Gauthier, I., Tarr, M.J., Moylan, J., Skudlarski, P., Gore, J.C., Anderson, A.W., 2000. The fusiform "face area" is part of a network that processes faces at the individual level. J. Cogn. Neurosci. 12 (3), 495–504.
Glasser, M.F., Coalson, T.S., Robinson, E.C., Hacker, C.D., Harwell, J., Yacoub, E., et al., 2016. A multi-modal parcellation of human cerebral cortex. Nature 536 (7615), 171–178.
Glomb, K., Mullier, E., Carboni, M., Rubega, M., Iannotti, G., Tourbier, S., et al., 2020a. Using structural connectivity to augment community structure in EEG functional connectivity. Netw. Neurosci. 4 (3), 1–27 May 20.
Glomb, K., Rué Queralt, J., Pascucci, D., Defferrard, M., Tourbier, S., Carboni, M., et al., 2020b. Connectome spectral analysis to track EEG task dynamics on a subsecond scale. Neuroimage 221, 117137 Nov.
Goodman, J.E., 2008. Surveys on Discrete and Computational Geometry: Twenty Years Later. American Mathematical Soc. AMS-IMS-SIAM Joint Summer Research ConferenceJune 18-22, 2006Vol. 453.
Gordon, E.M., Laumann, T.O., Adeyemo, B., Huckins, J.F., Kelley, W.M., Petersen, S.E., 2016. Generation and evaluation of a cortical area parcellation from resting-state correlations. Cereb. Cortex 26 (1), 288–303.
Grassi, F., Loukas, A., Perraudin, N., Ricaud, B., 2017. A time-vertex signal processing framework: scalable processing and meaningful representations for time-series on graphs. IEEE Trans. Signal Process. 66 (3), 817–829.
Griffa, A., Alemán-Gómez, Y., Hagmann, P., 2019. Structural and functional connectome from 70 young healthy adults [Data set]. Zenodo.
Haak, K.V., Beckmann, C.F., 2020. Understanding brain organisation in the face of functional heterogeneity and functional multiplicity. Neuroimage 220, 117061 Oct.
Hagmann, P., Cammoun, L., Gigandet, X., Meuli, R., Honey, C.J., Wedeen, V.J., et al., 2008. Mapping the structural core of human cerebral cortex. PLoS Biol. 6 (7), e159.
Hagmann, P., 2005. From diffusion MRI to brain connectomics (Doctoral dissertation). Ecole Polytechnique Fédérale de Lausanne (EPFL).
Hammond, D.K., Vandergheynst, P., Gribonval, R., 2011. Wavelets on graphs via spectral graph theory. Appl. Comput. Harmon. Anal. 30 (2), 129–150.
Hausmann, J.C., 1995. Others. On the vietoris-rips complexes and a cohomology theory for metric spaces. Ann. Math. Stud. 138, 175–188.
Haxby, J.V., Hoffman, E.A., Gobbini, M.I., 2000. The distributed human neural system for face perception. Trends Cogn. Sci. 4 (6), 223–233 (Regul. Ed.).

Hopfield, J.J., 1982. Neural networks and physical systems with emergent collective computational abilities. Proc. Natl. Acad. Sci. 79 (8), 2554–2558.
Huang, W., Goldsberry, L., Wymbs, N.F., Grafton, S.T., Bassett, D.S., Ribeiro, A., 2016. Graph frequency analysis of brain signals. IEEE J. Sel. Top. Signal Process 10 (7), 1189–1203.
Ito, T., Hearne, L.J., Cole, M.W., 2020. A cortical hierarchy of localized and distributed processes revealed via dissociation of task activations, connectivity changes, and intrinsic timescales. Neuroimage 221, 117141.
Johnson, M.H., 2005. Subcortical face processing. Nat. Rev. Neurosci. 6 (10), 766–774.
Kanwisher, N., McDermott, J., Chun, M.M., 1997. The fusiform face area: a module in human extrastriate cortex specialized for face perception. J. Neurosci. 17 (11), 4302–4311.
Leske, S., Dalal, S.S., 2019. Reducing power line noise in EEG and MEG data via spectrum interpolation. Neuroimage 189, 763–776.
Lioi, G., Gripon, V., Brahim, A., Rousseau, F., Farrugia, N., 2021. Gradients of connectivity as graph fourier bases of brain activity. Netw. Neurosci. 1–25 Jan 13.
Park, B., de Wael, R.V., Paquola, C., Larivière, S., Benkarim, O., Royer, J., et al., 2021. Signal diffusion along connectome gradients and inter-hub routing differentially contribute to dynamic human brain function. Neuroimage 224, 117429.
Pascucci, D., Tourbier, S., Rué-Queralt, J., Carboni, M., Hagmann, P., Plomp, G., 2021. Source imaging of high-density visual evoked potentials with multi-scale brain parcellations and connectomes [Internet]. Neuroscience doi:10.1101/2021.03.16.435599, Mar [cited 2021 Mar 22]. Available from.
Plomp, G., Michel, C.M., Herzog, M.H., 2010. Electrical source dynamics in three functional localizer paradigms. Neuroimage 53 (1), 257–267.
Preti, M.G., Van De Ville, D., 2019. Decoupling of brain function from structure reveals regional behavioral specialization in humans. Nat. Commun. 10 (1), 4747 Dec.
Raj, A., Cai, C., Xie, X., Palacios, E., Owen, J., Mukherjee, P., et al., 2020. Spectral graph theory of brain oscillations. Hum. Brain Mapp. 41 (11), 2980–2998.
Roberts, J.A., Perry, A., Lord, A.R., Roberts, G., Mitchell, P.B., Smith, R.E., et al., 2016. The contribution of geometry to the human connectome. Neuroimage 124, 379–393 Jan.
Robinson, P.A., Rennie, C.J., Rowe, D.L., O'Connor, S.C., Wright, J.J., Gordon, E., et al., 2003. Neurophysical modeling of brain dynamics. Neuropsychopharmacol. 28 (S1), S74–S79 Jul.
Rolls, E.T., 2007. The representation of information about faces in the temporal and frontal lobes. Neuropsychologia 45 (1), 124–143.
Rubega, M., Carboni, M., Seeber, M., Pascucci, D., Tourbier, S., Toscano, G., et al., 2019. Estimating EEG source dipole orientation based on singular-value decomposition for connectivity analysis. Brain Topogr. 32 (4), 704–719.
Rubinov, M., Sporns, O., 2010. Complex network measures of brain connectivity: uses and interpretations. Neuroimage 52 (3), 1059–1069 Sep.
Rué-Queralt, J., Stevner, A., Tagliazucchi, E., Laufs, H., Kringelbach, M.L., Deco, G., et al., 2021. Decoding brain states on the intrinsic manifold of human brain dynamics across wakefulness and sleep. Commun. Biol. 4 (1), 854 Dec.
Saggar, M., Sporns, O., Gonzalez-Castillo, J., Bandettini, P.A., Carlsson, G., Glover, G., et al., 2018. Towards a new approach to reveal dynamical organization of the brain using topological data analysis. Nat. Commun. 9 (1), 1–14.
Seguin, C., Tian, Y., Zalesky, A., 2020. Network communication models improve the behavioral and functional predictive utility of the human structural connectome. Netw. Neurosci. 4 (4), 980–1006 Jan.
Seung, H.S., 1996. How the brain keeps the eyes still. Proc. Natl. Acad. Sci. 93 (23), 13339–13344.
Shine, J.M., Breakspear, M., Bell, P.T., Martens, K.A.E., Shine, R., Koyejo, O., et al., 2019. Human cognition involves the dynamic integration of neural activity and neuromodulatory systems. Nat. Neurosci. 22 (2), 289 Feb.
Shuman, D.I., Narang, S.K., Frossard, P., Ortega, A., Vandergheynst, P., 2013. The emerging field of signal processing on graphs: extending high-dimensional data analysis to networks and other irregular domains. IEEE Signal Process. Mag. 30 (3), 83–98.
Sorrentino, P., Seguin, C., Rucco, R., Liparoti, M., Troisi Lopez, E., Bonavita, S., et al., 2021. The structural connectome constrains fast brain dynamics. Elife 10, e67400 Jul 9.
Sporns, O., Tononi, G., Kötter, R., 2005. The human connectome: a structural description of the human brain. PLoS Comput. Biol. 1 (4), e42.
Tononi, G., Sporns, O., Edelman, G.M., 1994. A measure for brain complexity: relating functional segregation and integration in the nervous system. Proc. Natl. Acad. Sci. 91 (11), 5033–5037.
Tourbier, S., Alemán-Gómez, Y., Mullier, E., Griffa, A., Cuadra, M.B., Hagmann, P., 2020. Connectomicslab/connectomemapper3: connectome mapper (version v3.0.0-beta-RC1). Zenodo.
Vault, M., 2021. The Definitive glossary of higher mathematical jargon — canonical [WWW Document]. https://mathvault.ca/math-glossary/#canonical (accessed 03.22.21)
Vincent, J.L., Patel, G.H., Fox, M.D., Snyder, A.Z., Baker, J.T., Van Essen, D.C., et al., 2007. Intrinsic functional architecture in the anaesthetized monkey brain. Nature 447 (7140), 83–86 May.
Virtanen, P., Gommers, R., Oliphant, T.E., Haberland, M., Reddy, T., Cournapeau, D., et al., 2020. SciPy 1.0: fundamental algorithms for scientific computing in python. Nat. Methods 17, 261–272.
Wang, R., Lin, P., Liu, M., Wu, Y., Zhou, T., Zhou, C., 2019. Hierarchical connectome modes and critical state jointly maximize human brain functional diversity. Phys. Rev. Lett. 123 (3), 038301.
Wedeen, V.J., Wang, R., Schmahmann, J.D., Benner, T., Tseng, W.-Y.I., Dai, G., et al., 2008. Diffusion spectrum magnetic resonance imaging (DSI) tractography of crossing fibers. Neuroimage 41 (4), 1267–1277.
Yeo, B.T., Krienen, F.M., Sepulcre, J., Sabuncu, M.R., Lashkari, D., Hollinshead, M., et al., 2011. The organization of the human cerebral cortex estimated by intrinsic functional connectivity. J. Neurophysiol. 106 (3), 1125.